Aberrant IP_3 receptor activities revealed by comprehensive analysis of pathological mutations causing spinocerebellar ataxia 29

Hideaki Ando[a,1,2], Matsumi Hirose[a], and Katsuhiko Mikoshiba[a,1]

[a]Laboratory for Developmental Neurobiology, RIKEN Center for Brain Science, Wako, Saitama 351-0198, Japan

Edited by Tullio Pozzan, University of Padova, Padova, Italy, and approved October 18, 2018 (received for review June 28, 2018)

Spinocerebellar ataxia type 29 (SCA29) is autosomal dominant congenital ataxia characterized by early-onset motor delay, hypotonia, and gait ataxia. Recently, heterozygous missense mutations in an intracellular Ca^{2+} channel, inositol 1,4,5-trisphosphate (IP_3) receptor type 1 (IP_3R1), were identified as a cause of SCA29. However, the functional impacts of these mutations remain largely unknown. Here, we determined the molecular mechanisms by which pathological mutations affect IP_3R1 activity and Ca^{2+} dynamics. Ca^{2+} imaging using IP_3R-null HeLa cells generated by genome editing revealed that all SCA29 mutations identified within or near the IP_3-binding domain of IP_3R1 completely abolished channel activity. Among these mutations, R241K, T267M, T267R, R269G, R269W, S277I, K279E, A280D, and E497K impaired IP_3 binding to IP_3R1, whereas the T579I and N587D mutations disrupted channel activity without affecting IP_3 binding, suggesting that T579I and N587D compromise channel gating mechanisms. Carbonic anhydrase-related protein VIII (CA8) is an IP_3R1-regulating protein abundantly expressed in cerebellar Purkinje cells and is a causative gene of congenital ataxia. The SCA29 mutation V1538M within the CA8-binding site of IP_3R1 completely eliminated its interaction with CA8 and CA8-mediated IP_3R1 inhibition. Furthermore, pathological mutations in CA8 decreased CA8-mediated suppression of IP_3R1 by reducing protein stability and the interaction with IP_3R1. These results demonstrated the mechanisms by which pathological mutations cause IP_3R1 dysfunction, i.e., the disruption of IP_3 binding, IP_3-mediated gating, and regulation via the IP_3R-modulatory protein. The resulting aberrant Ca^{2+} homeostasis may contribute to the pathogenesis of cerebellar ataxia.

spinocerebellar ataxia | calcium signaling | IP3 receptor | carbonic anhydrase-related protein VIII | missense mutation

Spinocerebellar ataxias (SCAs) are a group of clinically and genetically heterogeneous neurological disorders caused by cerebellar dysfunction (1). SCA type 29 (SCA29) is an autosomal dominant congenital nonprogressive ataxia characterized by early-onset gross motor delay, hypotonia, and gait ataxia. Affected individuals often have mild cognitive impairment and cerebellar atrophy (2). Recently, heterozygous missense mutations in inositol 1,4,5-trisphosphate (IP_3) receptor type 1 (IP_3R1) were identified in SCA29 (2–10). Deletion or missense mutations in IP_3R1 have also been identified in adult-onset, slowly progressive cerebellar ataxia SCA15/16 (10–13). IP_3R1 is a tetrameric Ca^{2+} channel located on intracellular Ca^{2+} stores such as the endoplasmic reticulum (ER). IP_3R1 is activated by binding to IP_3, a second messenger produced by hydrolysis of phosphatidylinositol 4,5-bisphosphate in response to the activation of cell surface receptors (14, 15). Among the three subtypes (IP_3R1, IP_3R2, and IP_3R3), IP_3R1 is the dominant subtype in the central nervous system and is highly expressed in cerebellar Purkinje cells (16). IP_3R1 knockout mice exhibit severe ataxia, dystonia, abnormal morphology of Purkinje cells, and impaired motor learning (17–20). IP_3Rs contain IP_3-binding domain near the N terminus, channel domain with six transmembrane regions close to the C terminus, and regulatory/coupling domain between them (15). Structural analyses indicated that IP_3 binding to IP_3R1 induces allosteric conformational changes in the channel (21–25). Eleven SCA29 missense mutations, R241K, T267M, T267R, R269G, R269W, S277I, K279E, A280D, E497K, T579I, and N587D (2–6, 8), and a putative SCA15 mutation, V479I (13), have been identified within or close to the IP_3-binding domain (26); however, the functional consequences of these mutations remain unknown.

Carbonic anhydrase-related protein VIII (CA8, also known as CARP) is a cytosolic protein abundantly expressed in cerebellar Purkinje cells (27, 28). CA8 interacts with the regulatory/coupling domain of IP_3R1 and inhibits IP_3 binding to IP_3R1 (29). CA8 is a causative gene of congenital ataxia and mental retardation and two missense mutations, S100P and G162R, have been identified in affected individuals (30, 31). The overlapping symptoms of human genetic diseases caused by mutations in IP_3R1 and CA8 suggest that aberrant IP_3R1 regulation via CA8 contributes to impaired motor coordination. Notably, the SCA29 mutation V1538M (2, 3, 7) and missense mutation S1478D identified in ataxic cerebral palsy with gross motor delay (32) are within the CA8-binding site in the regulatory/coupling domain of IP_3R1 (29).

Significance

Spinocerebellar ataxias (SCAs) are neurological disorders caused by cerebellar dysfunction. Missense mutations in inositol 1,4,5-trisphosphate (IP_3) receptor type 1 (IP_3R1), an IP_3-gated intracellular Ca^{2+} channel, are associated with infantile-onset nonprogressive SCA. However, the molecular mechanisms of how mutations in IP_3R1 cause SCA remain unclear. We demonstrated that pathological mutations in IP_3R1 disrupt IP_3R1 channel activity either by reducing IP_3-binding affinity or hindering channel gating elicited by IP_3 binding. Furthermore, disease-causing mutations in IP_3R1 or carbonic anhydrase-related protein VIII (CA8), an IP_3R1-regulating protein abundantly expressed in cerebellar neurons, abrogated the IP_3R1–CA8 interaction and CA8-mediated regulation of IP_3R1. These results suggest that aberrant calcium homeostasis in cerebellar neurons caused by dysfunctions of IP_3R1 are responsible for SCA pathogenesis.

Author contributions: H.A. and K.M. designed research; H.A. and M.H. performed research; H.A. and M.H. contributed new reagents/analytic tools; H.A. analyzed data; and H.A. wrote the paper.

The authors declare no conflict of interest.

This article is a PNAS Direct Submission.

[1]To whom correspondence may be addressed. Email: hideaki.ando@alum.riken.jp or mikosiba@brain.riken.jp.

[2]Present address: Laboratory of Molecular Biomedicine for Pathogenesis, Center for Disease Biology and Integrative Medicine, Faculty of Medicine, The University of Tokyo, Tokyo 113-0033, Japan.

This article contains supporting information online at www.pnas.org/lookup/suppl/doi:10.1073/pnas.1811129115/-/DCSupplemental.

Published online November 14, 2018.

However, the effects of these pathological mutations in IP_3R1 and CA8 on CA8-mediated IP_3R1 regulation remain unknown.

The functional impacts of two SCA mutations in IP_3R1 have been analyzed previously; the SCA15 mutation P1059L increases IP_3 affinity for IP_3R1, whereas it has no effects on Ca^{2+} release activity (33). The SCA29 mutation R36C causes gain-of-function of IP_3R1 activity with enhanced IP_3-binding affinity (9). However, more than 20 SCA15/29 mutations remain uncharacterized, mostly because analysis of IP_3R mutants is limited by the presence of endogenous IP_3R activity in nearly all cell types. Chicken B cell-derived DT40 cells in which all three IP_3R genes are deleted [DT40-triple knockout (TKO) cells] (34) have been utilized to characterize mutant IP_3R1 activity. However, DT40-TKO cells are not suitable for comprehensively analyzing human IP_3R1 mutants because of their low transfection efficiency and nonhuman origin. Here, we established human cervical cancer HeLa cells in which all three IP_3R genes were disrupted by CRISRP/Cas9 genome editing. The IP_3R triple knockout HeLa cells (HeLa-TKO cells) enabled the efficient analysis of the functional consequences of a majority of previously uncharacterized pathological mutations in IP_3R1. Additionally, we analyzed the effects of pathological mutations in CA8 on the regulation of IP_3R1. These analyses revealed the dramatic impacts of SCA29 mutations on IP_3 binding, gating, and CA8-mediated regulation of IP_3R1.

Results

Generation of IP_3R Triple Knockout HeLa Cells. For functional characterization of IP_3R1 containing SCA15/29 pathological mutations, we generated IP_3R-null HeLa cell lines lacking endogenous IP_3R activity. We disrupted all three IP_3R subtypes, IP_3R1, IP_3R2, and IP_3R3, by CRISPR/Cas9 genome editing using a high-fidelity Cas9 nuclease (35). We confirmed the knockout of IP_3Rs by Western blotting (Fig. 1*A*) and genomic analysis (*SI Appendix*, Fig. S1). We performed Ca^{2+} imaging to evaluate IP_3R activity. Wild-type or TKO HeLa cells were loaded with the Ca^{2+} indicator Fura-2 acetoxymethyl ester (AM) and stimulated with the IP_3-generating agonist histamine under extracellular Ca^{2+}-free conditions. IP_3-induced Ca^{2+} release was completely abolished in HeLa-TKO cells (Fig. 1*B*), confirming the lack of IP_3R activity. Treatment of the cells with thapsigargin, an inhibitor of SERCA Ca^{2+} pumps, showed that HeLa-TKO cells exhibited similar Ca^{2+} increases as in wild-type HeLa cells (Fig. 1*C*), indicating that the intracellular Ca^{2+} stores in HeLa-TKO cells were intact.

We constructed an expression vector encoding human IP_3R1 ($SI^-/SII^+/SIII^-$ splicing variant) (33) with an N-terminal mRFP-P2A tag. The peptide bond at the C terminus of the P2A peptide is cleaved in cells, and mRFP fluorescence can be used as a marker of transfected cells (36). We generated 14 missense mutants of human IP_3R1: R241K, T267M, T267R, R269G, R269W, S277I, K279E, A280D, V479I, E497K, T579I, N587D, S1478D, and V1538M, identified in SCA29, SCA15, and ataxic cerebral palsy (2–10, 13, 32) (Fig. 1*D*). mRFP-P2A-IP_3R1 mutants were efficiently expressed in HeLa-TKO cells by transient transfection (Fig. 1*E*). Immunostaining of the mRFP-P2A-IP_3R1 mutants expressed in HeLa-TKO cells clearly showed that all IP_3R1 mutants colocalized with the ER marker calnexin similar to wild-type IP_3R1 (*SI Appendix*, Fig. S2), indicating that these mutations did not disturb the ER distribution of IP_3R1.

Channel Activity of SCA IP_3R1 Mutants. We analyzed the channel activity of IP_3R1 mutants by Ca^{2+} imaging using HeLa-TKO cells. Cells transfected with mRFP-P2A-IP_3R1 mutants were loaded with Fura-2 AM and stimulated with histamine. Expression of wild-type IP_3R1, but not mock control, in HeLa-TKO cells restored the Ca^{2+} release activity in response to histamine (Fig. 2*A*). Interestingly, all SCA29 mutants of IP_3R1 containing a missense mutation within or close to the IP_3-binding domain, including R241K, T267M, T267R, R269G, R269W, S277I, K279E, A280D, E497K, T579I, and N587D, exhibited nearly no IP_3-induced Ca^{2+} release activity (Fig. 2*A*). In contrast, the SCA15 mutant V479I showed Ca^{2+} release to the same extent as wild-type IP_3R1. S1478D and V1538M, each carrying a mutation in the regulatory/coupling domain, also displayed comparative Ca^{2+} release to wild-type IP_3R1 (Fig. 2*A*). Quantification of the peak amplitude of Ca^{2+} release revealed clear all-or-none responses of the SCA mutants of IP_3R1 to agonist stimulation (Fig. 2*B*). Overexpression of IP_3R1 mutants did not alter the response to thapsigargin (Fig. 2*C*). These results suggest that the SCA29 mutations R241K, T267M, T267R, R269G, R269W, S277I, K279E, A280D, E497K, T579I, and N587D disrupted the channel activity of IP_3R1 in

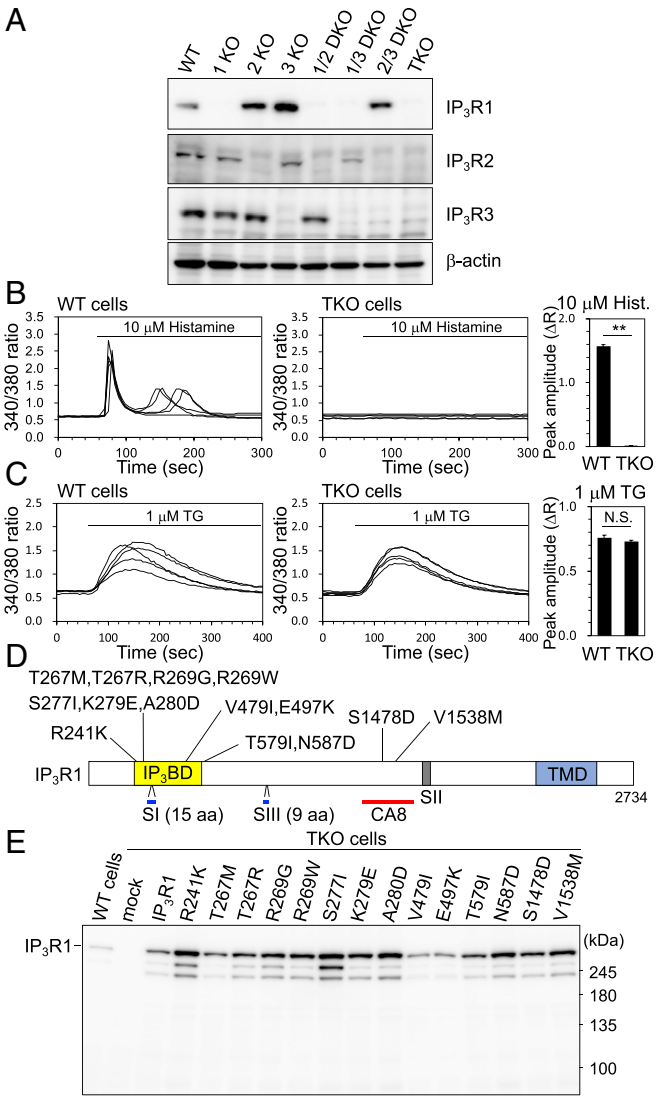

Fig. 1. IP_3R triple knockout HeLa cells and IP_3R1 mutants. (*A*) Western blotting of IP_3R single, double, or triple knockout HeLa cells. (*B* and *C*) Ca^{2+} imaging. Wild-type or TKO HeLa cells were loaded with Fura-2 AM and stimulated with 10 μM histamine (*B*) or 1 μM thapsigargin (*C*). Representative traces of the Fura-2 fluorescence ratio of five cells are shown. Bar graphs show peak amplitudes of Ca^{2+} transients (means ± SEM). (*B*) WT cells, n = 304; TKO cells, n = 319 from four independent experiments. (*C*) WT cells, n = 323; TKO cells, n = 296 from four independent experiments. $^{**}P < 0.01$ (Student's t test). (*D*) IP_3R1 SCA15/29 mutations analyzed in this study. IP_3-binding domain (IP_3BD), transmembrane domain (TMD), splice sites (SI, SII, and SIII), and CA-binding site (CA8) are shown. (*E*) HeLa-TKO cells transfected with mRFP-P2A (mock), mRFP-P2A-IP_3R1, or mRFP-P2A-IP_3R1 mutants were analyzed by Western blotting with anti-IP_3R1.

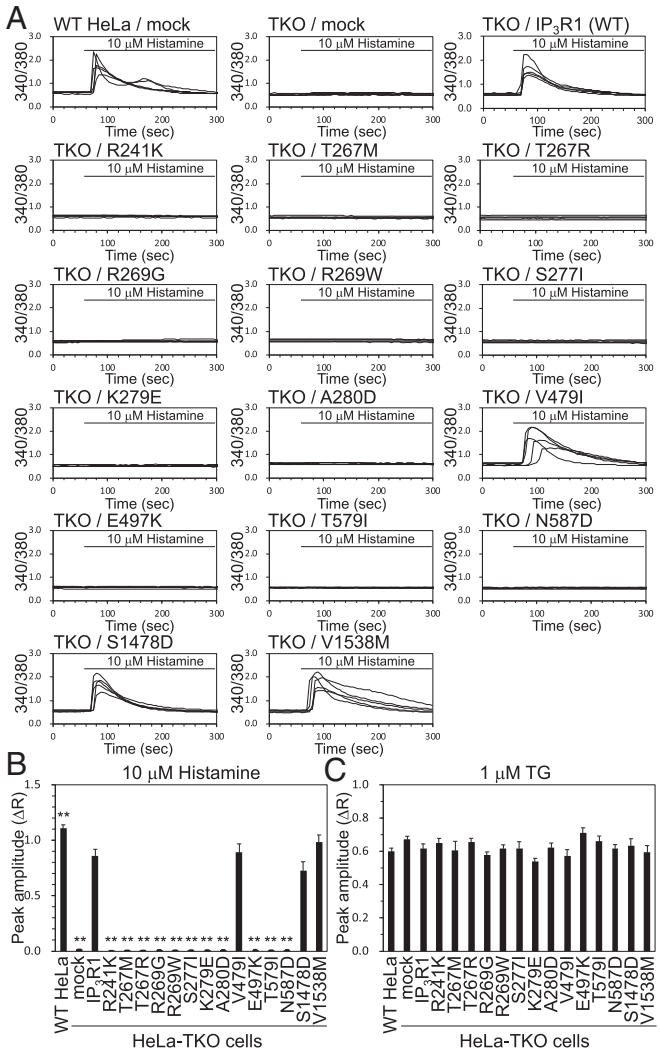

Fig. 2. IP_3-induced Ca^{2+} release activity of IP_3R1 mutants. (*A*) HeLa-TKO cells transfected with mRFP-P2A (mock), mRFP-P2A-IP_3R1, or mRFP-P2A-IP_3R1 mutants were loaded with Fura-2 AM and stimulated with 10 μM histamine. Representative traces of Fura-2 fluorescence ratio of five mRFP-positive cells are shown. (*B*) Peak amplitude of Ca^{2+} release induced by 10 μM histamine are shown as the mean ± SEM. Number of cells analyzed from at least three independent experiments; WT HeLa, $n = 242$; TKO cells, mock, $n = 108$; IP_3R1, $n = 87$; R241K, $n = 66$; T267M, $n = 56$; T267R, $n = 50$; R269G, $n = 35$; R269W, $n = 45$; S277I, $n = 45$; K279E, $n = 50$; A280D, $n = 58$; V479I, $n = 61$; E497K, $n = 52$; T579I, $n = 57$; N587D, $n = 57$; S1478D, $n = 50$; V1538M, $n = 59$. (*C*) Peak amplitude of Ca^{2+} transients induced by 1 μM thapsigargin are shown as the mean ± SEM. Number of cells analyzed from at least four independent experiments; WT HeLa, $n = 146$; TKO cells, mock, $n = 141$; IP_3R1, $n = 69$; R241K, $n = 68$; T267M, $n = 40$; T267R, $n = 78$; R269G, $n = 62$; R269W, $n = 73$; S277I, $n = 63$; K279E, $n = 57$; A280D, $n = 65$; V479I, $n = 38$; E497K, $n = 59$; T579I, $n = 68$; N587D, $n = 63$; S1478D, $n = 59$; V1538M, $n = 44$. $^{**}P < 0.01$ (one-way ANOVA followed by Dunnett's test, compared with TKO + IP_3R1).

HeLa-TKO cells. Cotransfection of wild-type IP_3R1 with these nonfunctional IP_3R1 mutants reduced the Ca^{2+} release activity (*SI Appendix*, Fig. S3), suggesting that incorporation of inactive mutant subunits into the IP_3R1 tetramer had dominant negative effects on the channel activation.

IP_3-Binding Activity of SCA IP_3R1 Mutants. We investigated the molecular mechanisms of how SCA29 mutations in IP_3R1 eliminated channel activity. Because 12 mutations (R241K, T267M, T267R, R269G, R269W, S277I, K279E, A280D, V479I, E497K, T579I, and N587D) are within or near the IP_3-binding domain of IP_3R1 (residues 226–563; corresponding residues 226–578 in mouse IP_3R1) (26), we tested whether these mutations affect IP_3-binding activity. Recombinant GST fusion proteins of the N-terminal 589 amino acids of IP_3R1, GST-IP_3R1-(1–589), containing an SCA mutation were purified (*SI Appendix*, Fig. S4*A*) and their [^{3}H]IP_3-binding activities were analyzed. R241K, T267M, T267R, R269G, R269W, S277I, K279E, A280D, and E497K showed prominently reduced IP_3 binding. In contrast, the V479I, T579I, and N587D mutants exhibited IP_3-binding activity comparative to that of wild-type GST-IP_3R1-(1–589) (Fig. 3*A*). We confirmed that the T579I and N587D mutations did not affect IP_3-binding activity using a larger recombinant protein, GST-IP_3R1-(1–700) (Fig. 3*B* and *SI Appendix*, Fig. S4*B*).

The X-ray crystal structure of the IP_3-binding domain of mouse IP_3R1 in complex with IP_3 (21, 25) shows that T267 and R269 are directly involved in the interaction with IP_3 (Fig. 3*C*), which is consistent with the impaired IP_3 binding in the T267M, T267R, R269G, and R269W mutants (Fig. 3*A*). Although R241, S277, K279, A280, and E497 are distributed throughout the primary structure, they come into proximity to form a cluster of mutation sites near the IP_3-binding pocket in the 3D structure. This mutation hotspot is adjacent to K493 and R496 (K508 and R511 in mouse IP_3R1), which interacts with IP_3 (21, 25)

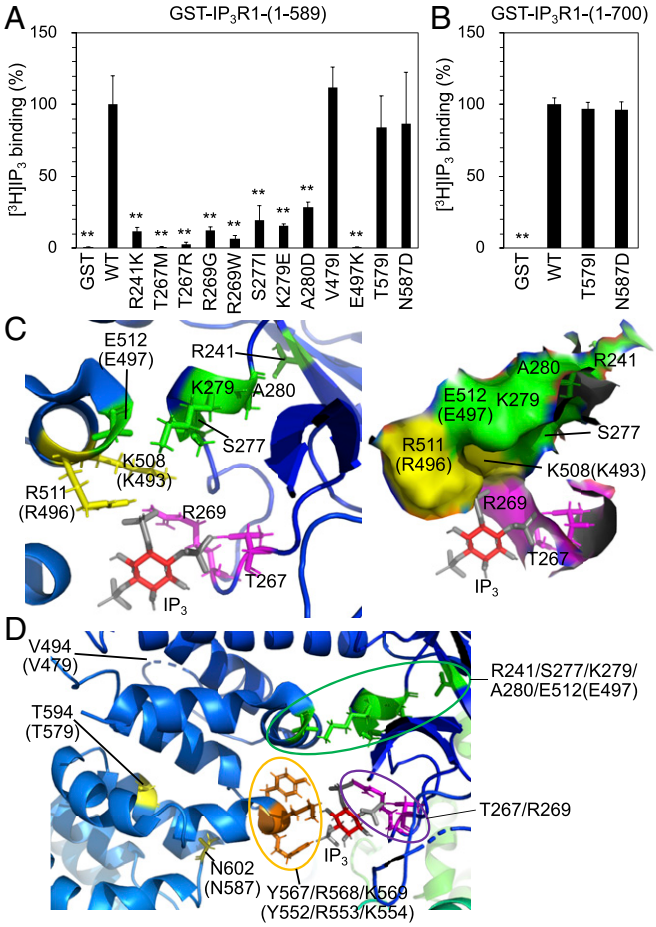

Fig. 3. IP_3-binding activity of IP_3R1 mutants. (*A* and *B*) Specific [^{3}H]IP_3 binding of GST-IP_3R1-(1–589) mutants (*A*) or GST-IP_3R1-(1–700) mutants (*B*) are shown as the mean ± SD ($n = 3$). $^{**}P < 0.01$ (one-way ANOVA followed by Dunnett's test, compared with WT). (*C* and *D*) Crystal structure of mouse IP_3R1-(1–2,217) in complex with IP_3 (25). Corresponding amino acid numbers in human IP_3R1 are shown in parentheses. V494 is in an unsolved region.

(Fig. 3*C*). This configuration may account for the drastic reduction of IP_3-binding activity in the R241K, S277I, K279E, A280D, and E497K mutants. Consistent with the normal IP_3-binding activity of the V479I, T579I, and N587D mutants (Fig. 3 *A* and *B*), V479, T579, and N587 are located away from the IP_3-binding core (Fig. 3*D*). In contrast to the V479I mutant, which showed normal IP_3-induced Ca^{2+} release activity, T579I and N587D displayed no channel activity (Fig. 2 *A* and *B*) despite their normal IP_3-binding activity. T579 and N587 are located near the α-helix containing Y552/R553/K554 (Y567/R568/K569 in mouse IP_3R1), which are involved in the interaction with IP_3 (21, 25) (Fig. 3*D*), suggesting that T579 and N587 are required for the IP_3-induced conformational change of the IP_3-binding domain.

Effects of Pathological Mutations in IP_3R1 on CA8-Mediated Regulation. Two pathological mutations, S1478D and V1538M, in the regulatory/coupling domain of IP_3R1 are located within the binding site of CA8 (residues 1373–1633) (29), a causative gene for cerebellar ataxia (30, 31). We analyzed the effects of the S1478D and V1538M mutations on the interaction between IP_3R1 and CA8. IP_3R1, S1478D, or V1538M were expressed in HeLa-TKO cells and the cell lysates were used for pulldown assays with GST-CA8. Notably, the V1538M mutation completely abolished the interaction with CA8 (Fig. 4*A*). Immunoprecipitation experiments also showed that HA-tagged CA8 interacted with wild-type IP_3R1 and the S1478D mutant, but not with the V1538M mutant in HeLa-TKO cells (Fig. 4*B*). Sequence alignment showed that V1538 in IP_3R1 is conserved in IP_3R2, whereas it is substituted by Met in IP_3R3 (*SI Appendix*, Fig. S5*A*). Analysis of the subtype specificity of CA8 binding showed that CA8 interacted with IP_3R1 and IP_3R2, but not with IP_3R3 (*SI Appendix*, Fig. S5 *B* and *C*), which is consistent with the failure of the V1538M mutant to bind to CA8. We analyzed the effects of CA8 overexpression on IP_3R activity by Ca^{2+} imaging. mRFP-P2A-CA8 significantly suppressed IP_3-induced Ca^{2+} release in 2/3 double KO (DKO) HeLa cells (Fig. 4*C*, *Top*), indicating that CA8 inhibited IP_3R1 activity. Although CA8 interacted with IP_3R2, CA8 did not suppress IP_3R2 (Fig. 4*C*, *Middle*). Consistent with the lack of interaction with IP_3R3, CA8 did not repress IP_3R3 (Fig. 4*C*, *Bottom*). Thus, CA8 specifically inhibits IP_3R1, but not IP_3R2 and IP_3R3.

Next, we investigated whether the S1478D and V1538M mutations affect CA8-mediated inhibition of IP_3R1. mRFP-P2A-IP_3R1, S1478D, or V1538M were transfected into HeLa-TKO cells with or without HA-CA8, and IP_3-induced Ca^{2+} release activity was measured. Exogenous IP_3R1 was suppressed by CA8 (Fig. 4*D*, *Top*), as was observed for endogenous IP_3R1 in 2/3 DKO HeLa cells (Fig. 4*C*, *Top*). Although S1478D was partially inhibited by CA8, the effect was not significant (Fig. 4*D*, *Middle*). Consistent with the lack of interaction (Fig. 4 *A* and *B*), the V1538M mutant was not suppressed by CA8 (Fig. 4*D*, *Bottom*). These results suggest that the S1478D and V1538M mutations abolished CA8-mediated suppression of IP_3R1 activity.

Effects of Pathological Mutations in CA8 on the IP_3R1 Regulation. Two missense mutations in the human CA8 gene, S100P and G162R, have been identified in individuals with cerebellar ataxia and mental retardation (30, 31). The S100P mutation has been shown to reduce the protein stability of CA8 without affecting its interaction with IP_3R1 (30); however, the biochemical properties of the G162R mutation remain unknown. Thus, we analyzed the protein stability of CA8 carrying the S100P or G162R mutation. We treated HeLa cells expressing mRFP-P2A-CA8, S100P, or G162R with the protein translation inhibitor cycloheximide (CHX). In contrast to wild-type CA8, which showed little degradation, S100P and G162R exhibited ~50% decreases in protein levels after 8 h of CHX treatment, suggesting that both the S100P and G162R mutations destabilize the CA8 protein (Fig. 5*A*).

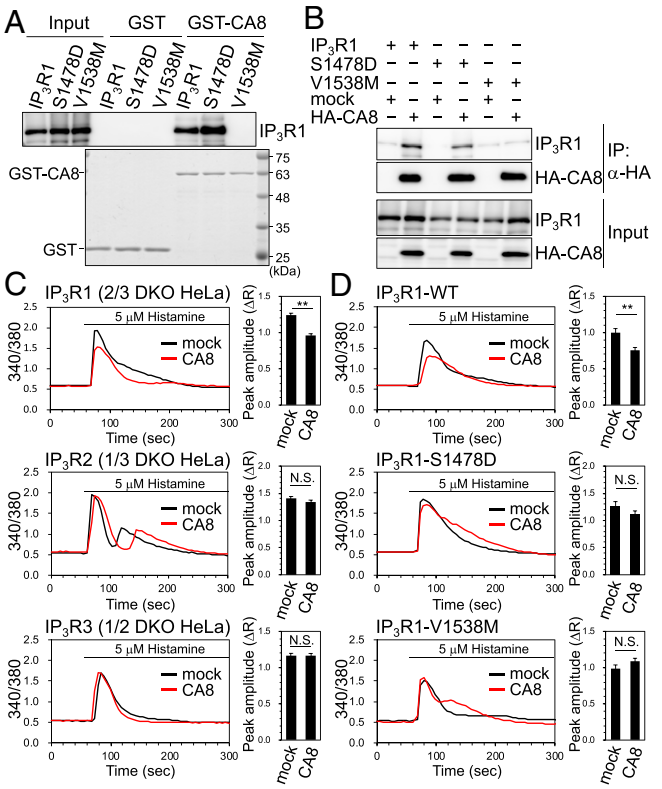

Fig. 4. Impacts of S1478D and V1538M mutations on CA8-mediated regulation of IP_3R1. (*A*) HeLa-TKO cells transfected with mRFP-P2A-IP_3R1, mRFP-P2A-IP_3R1-S1478D, or mRFP-P2A-IP_3R1-V1538M were processed for pulldown assay using GST or GST-CA8. Bound proteins were analyzed by Western blotting with anti-IP_3R1 or Coomassie Brilliant Blue (CBB) staining. (*B*) HeLa-TKO cells transfected with mRFP-P2A-IP_3R1, mRFP-P2A-IP_3R1-S1478D, or mRFP-P2A-IP_3R1-V1538M with or without HA-CA8 were processed for immunoprecipitation with anti-HA antibody. Immunoprecipitates were analyzed by Western blotting with anti-IP_3R1 and anti-HA. (*C*) 2/3 DKO (*Top*), 1/3 DKO (*Middle*), or 1/2 DKO (*Bottom*) HeLa cells were transfected with mRFP-P2A or mRFP-P2A-CA8. Cells were loaded with Fura-2 AM and stimulated with 5 μM histamine. Representative traces of Fura-2 fluorescence ratio of mRFP-positive cells are shown. Bar graphs show the peak amplitude of Ca^{2+} release represented as the mean ± SEM. Number of cells analyzed from four independent experiments; 2/3 DKO, mock, $n = 165$, CA8, $n = 171$; 1/3 DKO, mock, $n = 193$, CA8, $n = 186$; 1/2 DKO, mock, $n = 176$, CA8, $n = 189$. (*D*) HeLa-TKO cells were transfected with mRFP-P2A-IP_3R1 (*Top*), mRFP-P2A-IP_3R1-S1478D (*Middle*), or mRFP-P2A-IP_3R1-V1538M (*Bottom*) with mock or HA-CA8 (plasmid ratio 1:3). Cells were processed for Ca^{2+} imaging as described in *C*. Number of cells analyzed from seven independent experiments; IP_3R1 + mock, $n = 56$; IP_3R1 + CA8, $n = 71$; S1478D + mock, $n = 56$; S1478D + CA8, $n = 67$; V1538M + mock, $n = 68$; V1538M + CA8, $n = 76$. $^{**}P < 0.01$ (Student's *t* test).

Next, we investigated whether CA8 mutations affect its interaction with IP_3R1. Both pulldown and immunoprecipitation assays showed that the G162R mutation markedly reduced the binding of CA8 to IP_3R1 (Fig. 5 *B* and *C*). Considering that the S100P mutation did not affect the interaction with IP_3R1 in the pulldown assay (Fig. 5*B*) and blot overlay assay (30), the lack of interaction of S100P with IP_3R1 by immunoprecipitation may be related to the instability and low expression levels of the S100P protein (Fig. 5*C*). Finally, we analyzed the regulation of IP_3R1 activity by CA8 mutants by Ca^{2+} imaging using 2/3 DKO HeLa cells. Inhibition of IP_3R1 activity via CA8 was significantly attenuated by the G162R mutation (Fig. 5*D*). These results suggest that the G162R mutation abrogated CA8 function to suppress IP_3R1 by reducing the interaction with IP_3R1 and protein stability.

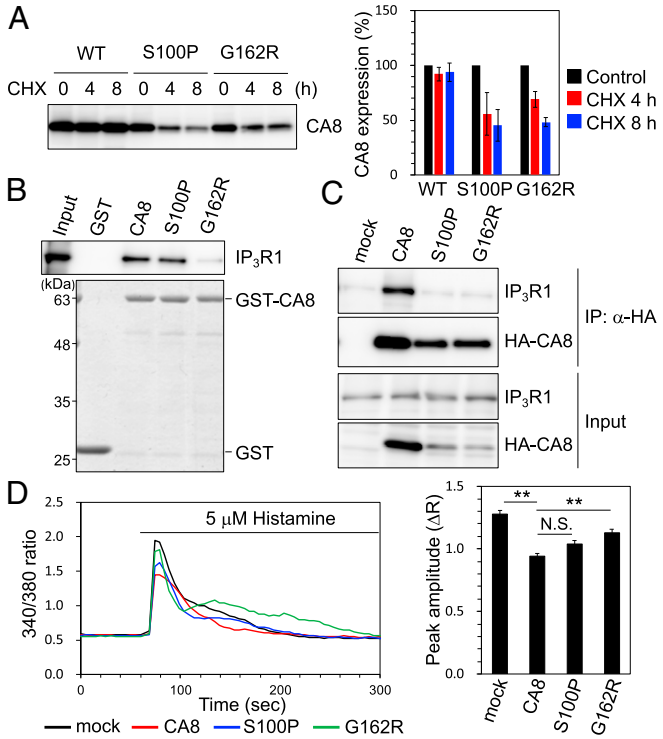

Fig. 5. Impacts of CA8 mutations on the regulation of IP_3R1. (*A*) HeLa cells transfected with mRFP-P2A-CA8, mRFP-P2A-CA8-S100P, or mRFP-P2A-CA8-G162R were treated with 50 μg/mL cycloheximide (CHX) for 0, 4, or 8 h. Expression levels of CA8 were analyzed by Western blotting with anti-CA8. Band intensities were represented as the mean ± SD ($n = 3$). (*B*) HeLa cell lysates were processed for pulldown assay using GST, GST-CA8, GST-CA8-S100P, or GST-CA8-G162R. Bound proteins were analyzed by Western blotting with anti-IP_3R1 or CBB staining. (*C*) HeLa cells transfected with mock, HA-CA8, HA-CA8-S100P, or HA-CA8-G162R were processed for immunoprecipitation with anti-HA antibody. Immunoprecipitates were analyzed by Western blotting with anti-IP_3R1 and anti-HA. (*D*) The 2/3 DKO HeLa cells were transfected with mRFP-P2A, mRFP-P2A-CA8, mRFP-P2A-CA8-S100P, or mRFP-P2A-CA8-G162R. Cells were loaded with Fura-2 AM and stimulated with 5 μM histamine. Representative traces of Fura-2 fluorescence ratio of mRFP-positive cells are shown. Bar graph shows peak amplitude of Ca^{2+} release represented as the mean ± SEM. Number of cells analyzed from four independent experiments; mock, $n = 146$, CA8, $n = 128$; CA8-S100P, $n = 157$, CA8-G162R, $n = 151$. $^{**}P < 0.01$ (one-way ANOVA followed by Tukey–Kramer test).

Discussion

We characterized the functional effects of missense mutations in IP_3R1 identified in SCA29 (R241K, T267M, T267R, R269G, R269W, S277I, K279E, A280D, E497K, T579I, N587D, and V1538M), SCA15 (V479I), and ataxic cerebral palsy (S1478D), and mutations in CA8 identified in congenital ataxia (S100P and G162R). The HeLa-TKO cells and DKO cells established in this study facilitated the analyses of mutant activities and subtype specificity of IP_3Rs, respectively. The analyses revealed that SCA29 mutations critically impair IP_3R1 channel activity or its CA8-mediated regulation.

The SCA29 mutations within or near the IP_3-binding domain: R241K, T267M, T267R, R269G, R269W, S277I, K279E, A280D, E497K, T579I, and N587D, completely disrupted the IP_3-induced Ca^{2+} release activity of IP_3R1. The entire loss of channel activity sharply contrasted the only previously characterized SCA29 mutation, R36C, which showed enhanced Ca^{2+} release activity (9) (*SI Appendix*, *SI Discussion*). The lack of channel activity in the R241K, T267M, T267R, R269G, R269W, S277I, K279E, A280D, and E497K mutants was due to impaired IP_3 binding. In contrast, the T579I and N587D mutations abolished IP_3R1 activity without affecting IP_3 binding. Crystallographic analyses of the N-terminal ~600 amino acids of rat IP_3R1 (22, 23) and ~2,200 amino acids of mouse IP_3R1 (25) in the presence or absence of IP_3 indicated that IP_3 binding induces allosteric conformational changes in the N-terminal cytoplasmic domain of IP_3R1. Considering that T579 and N587 are positioned adjacent to the α-helix containing Y552/R553/K554 which contacts the IP_3 molecule (21, 25), the T579I and N587D mutations may abrogate the IP_3-dependent conformation change of the IP_3-binding domain or its transmission to the channel domain. All of these mutations had dominant negative effects when coexpressed with wild-type IP_3R1. Since the IP_3R tetramer requires four IP_3 molecules to be activated (37), incorporation of mutant subunits lacking IP_3-binding activity or the IP_3-induced conformational changes in the IP_3R tetramer was assumed to inhibit the channel activation. This may explain earlier infantile onset of SCA29 compared with adult-onset SCA15/16, most of which are caused by haploinsufficiency of IP_3R1 due to heterozygous gene deletions (11–13). In contrast to SCA29 mutations, the V479I mutation identified in SCA15 (13) neither influenced channel activity nor IP_3 binding to IP_3R1 in this study. Considering that V479I has been identified in only a single individual to date, it may not be a pathogenic mutation. However, we cannot exclude the possibility that the V479I mutation affects the regulation by IP_3R1-interacting proteins.

CA8 is a cytosolic protein abundantly expressed in cerebellar Purkinje cells (27–29, 38). Homozygous missense mutations in CA8, S100P and G162R, are responsible for the syndrome with congenital ataxia and mild mental retardation with or without quadrupedal gait, respectively (30, 31). Additionally, a spontaneous 19-base pair deletion of the CA8 gene and loss of CA8 protein expression in Purkinje cells have been reported in waddles mice which exhibit ataxia, appendicular dystonia, and abnormal Purkinje cell synapses (38, 39). We demonstrated that pathological mutations in the CA8-binding region of IP_3R1, S1478D and V1538M, impaired CA8-mediated inhibition of IP_3R1. Furthermore, the S100P and G162R mutations in CA8 destabilized CA8 protein and G162R, but not S100P, reduced the interaction of CA8 with IP_3R1. Identification of disease-causing mutations in both IP_3R1 and CA8 that disrupt the IP_3R1–CA8 interaction strongly suggest that the failure of IP_3R1 regulation through CA8 leads to the pathogenesis of cerebellar ataxia. Structural analyses suggested that approximately half of the CA8-binding site containing S1478 and V1538 are in a structurally flexible region of IP_3R1 (24, 25). Because the CA8-binding site is distant from the IP_3-binding domain of the same subunit, CA8 may affect IP_3 binding to the adjacent subunit of the IP_3R1 tetramer. Alternatively, CA8 may regulate intersubunit transmission of conformation changes, which is suggested by electron cryomicroscopy analysis of the tetrameric IP_3R1 structure (24). However, we cannot exclude the possibility that CA8 mutations are involved in pathogenesis by other mechanisms in addition to IP_3R1 dysregulation. Besides, since S1478 and V1538 of IP_3R1 localize near a phosphorylation site by protein kinase A/G and a binding site of calmodulin (40), S1478D or V1538M mutation may also affect the IP_3R1 regulation via phosphorylation or Ca^{2+}/calmodulin. The pathological missense mutations in Gillespie syndrome (41–43) and anhidrosis (44) were identified in the C-terminal channel domain of IP_3R1 and IP_3R2, respectively. This suggests that these mutations directly affect the open–close transition of the channel domain or Ca^{2+} permeation through the channel pore. Our study demonstrated distinct mechanisms by which the pathological mutations impair IP_3R activity, namely the abrogation of IP_3 binding (R241K, T267M, T267R, R269G, R269W, S277I, K279E, A280D, and E497K), IP_3-mediated gating (T579I and N587D), and regulation through the IP_3R-accessory protein (S1478D and V1538M).

Recently, mutations in IP_3R1 were identified in Gillespie syndrome, a neural disease characterized by iris hypoplasia, nonprogressive cerebellar ataxia, hypotonia, and intellectual disability

(41–43). Furthermore, aberrant regulation of IP_3R1 through mutants ataxin-2 and ataxin-3 with polyglutamine expansion, which cause SCA2 and SCA3, respectively, has been demonstrated (45, 46). IP_3R1 and CA8 are highly expressed in cerebellar Purkinje cells (16, 27, 28), which play essential roles in cerebellar function by integrating input from parallel fibers and climbing fibers to transmit the sole output signal from the cerebellum to the deep cerebellar nuclei (10). Disturbances in Ca^{2+} homeostasis caused by dysfunction of IP_3R1 in Purkinje cells may contribute to defects in motor coordination. Indeed, mutations in Ca^{2+}-signaling molecules upstream or downstream of IP_3R1 have been identified in other types of SCA, including metabolic glutamate receptor 1 (47), protein kinase Cγ (48), and transient receptor potential channel 3 (49), all of which are highly expressed in Purkinje cells.

In summary, we comprehensively analyzed the functional impacts of pathological mutations in IP_3R1 and revealed that SCA29 mutations cause IP_3R1 dysfunction by impairing IP_3 binding, gating, or CA8-mediated regulation. Aberrant Ca^{2+} homeostasis caused by abnormal IP_3R1 activity may contribute to the molecular pathogenesis of SCA29.

Materials and Methods

Detailed description of plasmids, cell culture, transfection, CRISPR-mediated gene targeting, Ca^{2+} imaging, recombinant proteins, IP_3-binding assay, pulldown assay, and immunoprecipitation are provided in *SI Appendix, SI Materials and Methods*.

ACKNOWLEDGMENTS. We thank Drs. Kozo Hamada, Chihiro Hisatsune, and Katsuhiro Kawaai for valuable discussions and the RIKEN Center for Brain Science Research Resources Division for DNA sequencing analysis and common use facilities in the radioisotope center. This study was supported by the Japan Society for the Promotion of Science Grant-in-Aid for Scientific Research S 25221002 (to K.M.), Scientific Research C 18K06540 (to H.A.), and RIKEN Incentive Research Projects (H.A.).

1. Matilla-Dueñas A, et al. (2014) Consensus paper: Pathological mechanisms underlying neurodegeneration in spinocerebellar ataxias. *Cerebellum* 13:269–302.
2. Zambonin JL, et al.; Care4Rare Canada Consortium (2017) Spinocerebellar ataxia type 29 due to mutations in ITPR1: A case series and review of this emerging congenital ataxia. *Orphanet J Rare Dis* 12:121.
3. Huang L, et al. (2012) Missense mutations in ITPR1 cause autosomal dominant congenital nonprogressive spinocerebellar ataxia. *Orphanet J Rare Dis* 7:67.
4. Ohba C, et al. (2013) Diagnostic utility of whole exome sequencing in patients showing cerebellar and/or vermis atrophy in childhood. *Neurogenetics* 14:225–232.
5. Fogel BL, et al. (2014) Exome sequencing in the clinical diagnosis of sporadic or familial cerebellar ataxia. *JAMA Neurol* 71:1237–1246.
6. Sasaki M, et al. (2015) Sporadic infantile-onset spinocerebellar ataxia caused by missense mutations of the inositol 1,4,5-triphosphate receptor type 1 gene. *J Neurol* 262: 1278–1284.
7. Shadrina MI, et al. (2016) ITPR1 gene p.Val1553Met mutation in Russian family with mild spinocerebellar ataxia. *Cerebellum Ataxias* 3:2.
8. Barresi S, et al. (2017) Mutations in the IRBIT domain of ITPR1 are a frequent cause of autosomal dominant nonprogressive congenital ataxia. *Clin Genet* 91:86–91.
9. Casey JP, et al. (2017) A novel gain-of-function mutation in the ITPR1 suppressor domain causes spinocerebellar ataxia with altered Ca^{2+} signal patterns. *J Neurol* 264: 1444–1453.
10. Hisatsune C, Hamada K, Mikoshiba K (May 16, 2018) Ca^{2+} signaling and spinocerebellar ataxia. *Biochim Biophys Acta Mol Cell Res*, 10.1016/j.bbamcr.2018.05.009.
11. van de Leemput J, et al. (2007) Deletion at ITPR1 underlies ataxia in mice and spinocerebellar ataxia 15 in humans. *PLoS Genet* 3:e108.
12. Hara K, et al. (2008) Total deletion and a missense mutation of ITPR1 in Japanese SCA15 families. *Neurology* 71:547–551.
13. Ganesamoorthy D, et al. (2009) Development of a multiplex ligation-dependent probe amplification assay for diagnosis and estimation of the frequency of spinocerebellar ataxia type 15. *Clin Chem* 55:1415–1418.
14. Berridge MJ (2016) The inositol trisphosphate/calcium signaling pathway in health and disease. *Physiol Rev* 96:1261–1296.
15. Mikoshiba K (2007) IP_3 receptor/Ca^{2+} channel: From discovery to new signaling concepts. *J Neurochem* 102:1426–1446.
16. Furuichi T, et al. (1989) Primary structure and functional expression of the inositol 1,4,5-trisphosphate-binding protein P400. *Nature* 342:32–38.
17. Matsumoto M, et al. (1996) Ataxia and epileptic seizures in mice lacking type 1 inositol 1,4,5-trisphosphate receptor. *Nature* 379:168–171.
18. Hisatsune C, et al. (2006) Inositol 1,4,5-trisphosphate receptor type 1 in granule cells, not in Purkinje cells, regulates the dendritic morphology of Purkinje cells through brain-derived neurotrophic factor production. *J Neurosci* 26:10916–10924.
19. Hisatsune C, et al. (2013) IP3R1 deficiency in the cerebellum/brainstem causes basal ganglia-independent dystonia by triggering tonic Purkinje cell firings in mice. *Front Neural Circuits* 7:156.
20. Sugawara T, et al. (2013) Type 1 inositol trisphosphate receptor regulates cerebellar circuits by maintaining the spine morphology of purkinje cells in adult mice. *J Neurosci* 33:12186–12196.
21. Bosanac I, et al. (2002) Structure of the inositol 1,4,5-trisphosphate receptor binding core in complex with its ligand. *Nature* 420:696–700.
22. Lin CC, Baek K, Lu Z (2011) Apo and $InsP_3$-bound crystal structures of the ligand-binding domain of an $InsP_3$ receptor. *Nat Struct Mol Biol* 18:1172–1174.
23. Seo MD, et al. (2012) Structural and functional conservation of key domains in $InsP_3$ and ryanodine receptors. *Nature* 483:108–112.
24. Fan G, et al. (2015) Gating machinery of $InsP_3R$ channels revealed by electron cryomicroscopy. *Nature* 527:336–341.
25. Hamada K, Miyatake H, Terauchi A, Mikoshiba K (2017) IP_3-mediated gating mechanism of the IP_3 receptor revealed by mutagenesis and X-ray crystallography. *Proc Natl Acad Sci USA* 114:4661–4666.
26. Yoshikawa F, et al. (1996) Mutational analysis of the ligand binding site of the inositol 1,4,5-trisphosphate receptor. *J Biol Chem* 271:18277–18284.
27. Kato K (1990) Sequence of a novel carbonic anhydrase-related polypeptide and its exclusive presence in Purkinje cells. *FEBS Lett* 271:137–140.
28. Taniuchi K, Nishimori I, Takeuchi T, Ohtsuki Y, Onishi S (2002) cDNA cloning and developmental expression of murine carbonic anhydrase-related proteins VIII, X, and XI. *Brain Res Mol Brain Res* 109:207–215.
29. Hirota J, Ando H, Hamada K, Mikoshiba K (2003) Carbonic anhydrase-related protein is a novel binding protein for inositol 1,4,5-trisphosphate receptor type 1. *Biochem J* 372:435–441.
30. Türkmen S, et al. (2009) CA8 mutations cause a novel syndrome characterized by ataxia and mild mental retardation with predisposition to quadrupedal gait. *PLoS Genet* 5:e1000487.
31. Kaya N, et al. (2011) Phenotypical spectrum of cerebellar ataxia associated with a novel mutation in the CA8 gene, encoding carbonic anhydrase (CA) VIII. *Am J Med Genet B Neuropsychiatr Genet* 156B:826–834.
32. Parolin Schnekenberg R, et al. (2015) De novo point mutations in patients diagnosed with ataxic cerebral palsy. *Brain* 138:1817–1832.
33. Yamazaki H, et al. (2011) Functional characterization of the P1059L mutation in the inositol 1,4,5-trisphosphate receptor type 1 identified in a Japanese SCA15 family. *Biochem Biophys Res Commun* 410:754–758.
34. Sugawara H, Kurosaki M, Takata M, Kurosaki T (1997) Genetic evidence for involvement of type 1, type 2 and type 3 inositol 1,4,5-trisphosphate receptors in signal transduction through the B-cell antigen receptor. *EMBO J* 16:3078–3088.
35. Kleinstiver BP, et al. (2016) High-fidelity CRISPR-Cas9 nucleases with no detectable genome-wide off-target effects. *Nature* 529:490–495.
36. Kawaai K, et al. (2017) Splicing variation of Long-IRBIT determines the target selectivity of IRBIT family proteins. *Proc Natl Acad Sci USA* 114:3921–3926.
37. Alzayady KJ, et al. (2016) Defining the stoichiometry of inositol 1,4,5-trisphosphate binding required to initiate Ca^{2+} release. *Sci Signal* 9:ra35.
38. Jiao Y, et al. (2005) Carbonic anhydrase-related protein VIII deficiency is associated with a distinctive lifelong gait disorder in waddles mice. *Genetics* 171:1239–1246.
39. Hirasawa M, et al. (2007) Carbonic anhydrase related protein 8 mutation results in aberrant synaptic morphology and excitatory synaptic function in the cerebellum. *Mol Cell Neurosci* 35:161–170.
40. Foskett JK, White C, Cheung KH, Mak DO (2007) Inositol trisphosphate receptor Ca^{2+} release channels. *Physiol Rev* 87:593–658.
41. McEntagart M, et al.; DDD Study (2016) A restricted repertoire of de novo mutations in *ITPR1* cause Gillespie syndrome with evidence for dominant-negative effect. *Am J Hum Genet* 98:981–992.
42. Gerber S, et al. (2016) Recessive and dominant de novo *ITPR1* mutations cause Gillespie syndrome. *Am J Hum Genet* 98:971–980.
43. Dentici ML, et al. (2017) Identification of novel and hotspot mutations in the channel domain of ITPR1 in two patients with Gillespie syndrome. *Gene* 628:141–145.
44. Klar J, et al. (2014) Abolished $InsP_3R2$ function inhibits sweat secretion in both humans and mice. *J Clin Invest* 124:4773–4780.
45. Chen X, et al. (2008) Deranged calcium signaling and neurodegeneration in spinocerebellar ataxia type 3. *J Neurosci* 28:12713–12724.
46. Liu J, et al. (2009) Deranged calcium signaling and neurodegeneration in spinocerebellar ataxia type 2. *J Neurosci* 29:9148–9162.
47. Guergueltcheva V, et al. (2012) Autosomal-recessive congenital cerebellar ataxia is caused by mutations in metabotropic glutamate receptor 1. *Am J Hum Genet* 91: 553–564.
48. Chen DH, et al. (2003) Missense mutations in the regulatory domain of PKC gamma: A new mechanism for dominant nonepisodic cerebellar ataxia. *Am J Hum Genet* 72: 839–849.
49. Fogel BL, Hanson SM, Becker EB (2015) Do mutations in the murine ataxia gene TRPC3 cause cerebellar ataxia in humans? *Mov Disord* 30:284–286.